MODELING LEAKING GAS PLUME MIGRATION

DMITRIY SILIN, TAD PATZEK, AND SALLY M. BENSON

Abstract. In this study, we obtain simple estimates of 1-D plume propagation velocity taking into account the density and viscosity contrast between CO_2 and brine. Application of the Buckley-Leverett model to describe buoyancy-driven countercurrent flow of two immiscible phases leads to a transparent theory predicting the evolution of the plume. We obtain that the plume does not migrate upward like a gas bubble in bulk water. Rather, it stretches upward until it reaches a seal or until the fluids become immobile. A simple formula requiring no complex numerical calculations describes the velocity of plume propagation. This solution is a simplification of a more comprehensive theory of countercurrent plume migration that does not lend itself to a simple analytical solution (Silin *et al.*, 2006). The range of applicability of the simplified solution is assessed and provided.

This work is motivated by the growing interest in injecting carbon dioxide into deep geological formations as a means of avoiding its atmospheric emissions and consequent global warming. One of the potential problems associated with the geologic method of sequestration is leakage of CO_2 from the underground storage reservoir into sources of drinking water. Ideally, the injected green-house gases will stay in the injection zone for a geologically long time and eventually will dissolve in the formation brine and remain trapped by mineralization. However, naturally present or inadvertently created conduits in the cap rock may result in a gas leak from primary storage. Even in supercritical state, the carbon dioxide viscosity and density are lower than those of the indigenous formation brine. Therefore, buoyancy will tend to drive the CO_2 upward unless it is trapped beneath a low permeability seal. Theoretical and experimental studies of buoyancy-driven supercritical CO_2 flow, including estimation of time scales associated with plume evolution, are critical for developing technology, monitoring policy, and regulations for carbon dioxide geologic sequestration protecting the sources of potable water.

Dmitriy Silin is a geological scientist at the Earth Sciences Division of Ernest Orlando Lawrence Berkeley National Laboratory. He holds a degree of Doctor of Physical and Mathematical Sciences in applied mathematics from the Department of Computational Mathematics and Cybernetics of the same university. His research interests include mathematical models in geosciences including fluid flow and rock physics at different scales.

Tad Patzek is a professor of Geoengineering at U.C. Berkeley. Prior to joining Berkeley in 1990, he was a researcher at Shell Development, where he worked on the enhanced oil recovery methods and evaluated the future of U.S. energy supply from unconventional oil reservoirs, tar sands, heavy oil, oil shale, and coal. His current research involves mathematical modeling of earth systems with emphasis on fluid flow in soils and rocks. He is also working on the thermodynamics and ecology of human survival and energy supply schemes for humanity. Currently, he teaches courses in hydrology, ecology and energy supply, computer science, and mathematical modeling of earth systems at micro and mega scales.

Sally M. Benson is a Professor (Research) in the Energy Resources Engineering Department in the School of Earth Sciences at Stanford University and the Executive Director of the Global Climate and Energy Project. She joined Stanford in 2007 after working at Lawrence Berkeley National Laboratory in a number of capacities, including Earth Science Division Director, Associate Laboratory Director for Energy Sciences, and Deputy Director for Operations. She holds a M.S. and Ph.D. from the University of California in Materials Science and Mineral Engineering.

1. Introduction

The objective of this study is to obtain simple estimates of plume propagation velocity taking into account the density and viscosity contrast. This work follows previous studies (Silin et al., 2006, 2007) where a general model of two-phase vertical countercurrent flow has been discussed. Here, we simplify that model by neglecting capillary forces. This simplification leads to a more transparent theory while preserving the main conclusion of the more general approach. The theory predicts that in a porous medium, the plume does not migrate upward like a gas bubble in bulk water. Rather, it stretches upward until it reaches the surface or a uniform immobile gas saturation. Moreover, the simplified model discussed here predicts the same plume propagation velocity estimates as the model studied by Silin et al. (2007). Mathematically, the evolution of the plume can be characterized as a sequence of exact solutions usually called shock and rarefaction waves.

We adopt the following convention: the injected supercritical carbon dioxide will be called gas. We apply a hyperbolic approximation of the two-phase flow equation in a homogeneous reservoir. This approach admits an extension to heterogeneous media. In particular, we consider propagation of the front end of the plume through a layered formation. The theory predicts that a low-permeability layer significantly reduces the speed of propagation in all overlaying strata.

We believe that the theory developed here is provides reasonable estimates of the time of plume propagation from effective formation flow properties. Field and experimental work will help to scale and calibrate the most important parameters.

This work is motivated by the growing interest in injecting carbon dioxide into deep geological formations as a means of avoiding its atmospheric emissions and consequent global warming. Ideally, the injected gas will stay in the injection zone for a long time and will be dissolved in the formation brine and trapped by mineralization. However, a gas leak from primary storage may occur because of cracks or other naturally or inadvertently man-made conduits in the cap rock. Even if the injected carbon dioxide is in supercritical state, its viscosity and density are lower than those of the indigenous formation brine. Therefore, the buoyancy will always drive the injected carbon dioxide upward. Understanding the buoyancy-driven plume migration and estimation of the time scales associated with plume evolution are critical for developing appropriate regulations providing for the safety of potable water resources.

2. The model

A carbon dioxide plume migration involves various complex processes acting in different time scales. Juanes et al. (2006) formulate five principal mechanisms of CO_2 trapping: hydrodynamic trapping, solution trapping, mineral trapping, capillary trapping, and two-phase flow hysteresis. The latter is a consequence of gas trapping by water imbibing in water-wet rocks, (Al-Futaisi and Patzek, 2003; Valvante and Blunt, 2004).

In this work, we focus on buoyancy-driven two-phase viscous flow with account for hysteresis of relative permeabilities. This choice is based on the assumption that other processes, like dissolution and geochemistry are much slower than the flow. A leaking plume loses carbon dioxide at a certain rate as it migrates under buoyancy. Such losses only can slow down the plume propagation, so the case presented here can be qualified as the worst-case scenario.

2.1. Buckley–Leverett model of two-phase flow.

We assume that the plume crosses a thick aquifer with uniform flow properties. Let the vertical coordinate, z, be directed upward. Then a negative numerical value of Darcy velocity means flow downward, and a positive value means flow upward. Darcy's law for

two-phase flow states the following relationships between the Darcy velocities of gas and brine and their respective pressure gradients (Muskat, 1949; Hubbert, 1956):

$$u_g = -\frac{k_{rg}(S)k}{\mu_g}\left(\frac{\partial p_g}{\partial z} - \varrho_g g\right) \tag{1}$$

$$u_w = -\frac{k_{rw}(S)k}{\mu_w}\left(\frac{\partial p_w}{\partial z} - \varrho_w g\right) \tag{2}$$

Here u_g and u_w are Darcy velocities, or volumetric fluxes, of the gas and liquid, μ_g and μ_w are the dynamic viscosities of the fluids, p_g and p_w, and ϱ_g and ϱ_w are their pressures and densities, respectively. The brine volumetric saturation and gravity acceleration are denoted by S and g, and k is the absolute permeability of the medium. In this derivation, we neglect the compressibility of brine and supercritical gas. Since there is no sink or source of gas or brine, the flow is countercurrent:

$$u_g + u_w = 0 \tag{3}$$

To obtain equations in dimensionless form, we introduce dimensionless vertical coordinate ζ and time τ:

$$\zeta = \frac{z}{H} \qquad \tau = \frac{k\,(\varrho_w - \varrho_g)\,g}{\mu_w H}\,t \tag{4}$$

Here H is the thickness of the reservoir. A dimensionless formulation helps to single out the most important parameters and to simplify the model by dropping insignificant terms. Silin et al. (2006) have obtained that the contribution of the capillary pressure in the flow dynamics is negligible if

$$\left|\gamma \mathcal{J}'(S)\frac{\partial S}{\partial \zeta}\right| \ll 1 \tag{5}$$

where

$$\gamma = \frac{\sigma}{(\varrho_w - \varrho_g)gH}\sqrt{\frac{\phi}{k}} \tag{6}$$

is an analog of the reciprocal Bond number. In what follows, we assume that condition (5) holds true and the impact of capillarity can be neglected. Combination of Darcy's law with conservation of mass yields a hyperbolic equation for brine saturation S:

$$\phi\frac{\partial S}{\partial \tau} - \frac{\partial}{\partial \zeta}f(S) = 0 \tag{7}$$

where

$$f(S) = \frac{k_{rw}(S)}{\dfrac{k_{rw}(S)}{k_{rg}(S)}\dfrac{\mu_g}{\mu_w} + 1} \tag{8}$$

is the partial flow function. Equation (7) constitutes a Buckley–Leverett type flow model (Buckley and Leverett, 1942) in dimensionless form. It is interesting to note that the dimensionless Darcy velocity of brine

$$W_w = \frac{\mu_w}{k(\varrho_w - \varrho_g)g}u_w \tag{9}$$

equals minus partial flow function:

$$W_w = -f(S) \tag{10}$$

and the gravity acceleration enters the model through the time scale (4) only.

2.2. **Shock and rarefaction wave solutions.** A solution to a hyperbolic equation like Equation (7) propagates along characteristics (Petrovskii, 1966; Lax, 1973). Two types of stable saturation profiles develop. Using the terminology borrowed from gas dynamics (Landau and Lifshitz, 1959), such solutions are called shock and rarefaction waves. The first type characterizes a solution with abrupt variation of the saturation profile over a negligibly short distance. The second one characterizes a smoothly spreading solution.

If S_1 and S_2 are the saturations before and behind a shock wave, then mass conservation yields the following expression for the dimensionless shock propagation velocity

$$V_s(S_1, S_2) = -\frac{1}{\phi}\frac{f(S_2) - f(S_1)}{S_2 - S_1} \tag{11}$$

Note that the expression on the right-hand side can be either positive or negative, or can be equal to zero for an equilibrium saturation transition.

A rarefaction-wave solution is provided by the implicit relationship

$$\zeta = \zeta_0 - \tau\frac{1}{\phi}f'\left(S(\tau, \zeta)\right) \tag{12}$$

where ζ_0 is a parameter characterizing the location of the center of the wave. In particular, the velocity of propagation of the part of the rarefaction wave, where brine saturation S is equal to

$$V_r(S) = -\frac{1}{\phi}f'\left(S\right) \tag{13}$$

A rarefaction-wave solution depends on τ and ζ through a similarity variable

$$\eta = \frac{\zeta - \zeta_0}{\tau} \tag{14}$$

Due to the nature of wave propagation, in either case it is natural to express the solution in the form $\zeta = \zeta(S, \tau)$, rather than $S = S(\tau, \zeta)$.

To guarantee mass conservation at a transition between a shock wave and a rarefaction wave, both must have equal velocities of propagation

$$f'\left(S_i\right) = \frac{f(S_2) - f(S_1)}{S_2 - S_1} \tag{15}$$

where i is either 1 or 2.

3. Results and Discussion

We begin with describing evolution of the plume in a homogeneous formation. The plume can be described through a sequence of shock and rarefaction waves. On the top, the fastest propagating shock wave is lean with respect to gas saturation. The main part of the plume practically stays put, being reduced from the top part by the leading propagating front. In the following subsections, we present a description of the evolution of different parts of the plume using the two-phase buoyancy-driven flow theory developed above. For simplicity, we consider an initial plume with a constant gas saturation. We put the origin at the top of the initial plume (Figure 1).

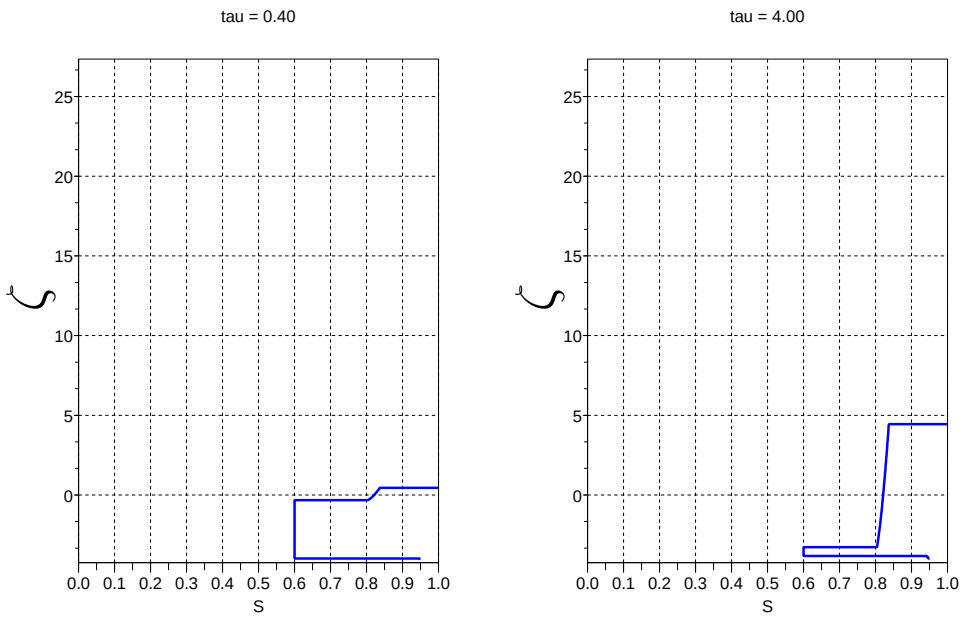

FIGURE 1. Vertical brine saturation profile at the early phase of plume evolution. The initial saturation of gas is 40 %. A leading front of low gas saturation propagates upward, whereas the main part of the plume gradually shrinks.

3.1. **The leading front of the plume.** In estimating the plume propagation time, the most critical part is the top leading edge of the plume. Assuming that the brine saturation ahead of the plume is one, Equations (4) and (11) imply that

$$V^* = \frac{1}{\phi}\frac{f(S^*)}{1-S^*} \tag{16}$$

is a dimensionless expression of the front propagation velocity. In physical units,

$$v^* = \frac{k(\varrho_w - \varrho_g)g}{\phi\mu_w}\frac{f(S^*)}{1-S^*} \tag{17}$$

This leading travelling-wave evolution of the saturation profile is followed by a rarefaction wave centered at the original location of the top part of the plume.

3.2. **Evolution of the main part of the plume.** Analysis of characteristics suggests that the evolution of the saturation profile behind the leading part of the plume, which has been described in the previous subsection, can be characterized as a sequence of two rarefaction and shock waves. Figures 1–3 display the profiles at different times in dimensionless units. The theory suggests that there are three time stages of plume evolution. At early time, the high-gas-saturation part of the plume thins between two traveling waves propagating in opposite directions (Figure 1). On the top, a travelling wave propagates downward to compensate for the flow of gas through the leading part. At early times, the travelling wave at the bottom of the plume propagates extremely slowly. This traveling wave is proceeded by a slowly-developing rarefaction wave. The latter is practically unnoticeable in the plots. The slow propagation is due to the

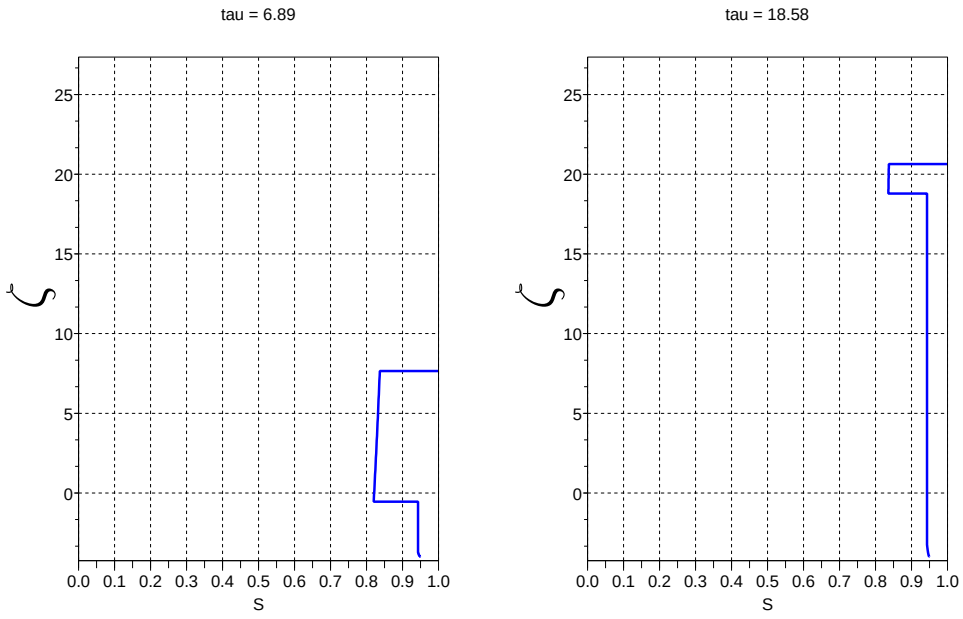

FIGURE 2. Evolution of the plume after its main part collapses. The lean leading part of the plume migrates upward whereas gas saturation behind it approaches the residual saturation.

very slow fluid exchange rate at a high gas saturation. This slow flow, in particular, is a consequence of the water-wet environment. As the wetting fluid, water flows through the corners and crevices in the pores. Therefore the permeability to brine drops dramatically in the presence of gas. The high (relative to the gas) water viscosity only further slows down fluid exchange.

This travelling wave at the bottom is so slow that, due to roundoff errors, numerical simulations may entirely miss it along with the following traveling wave (Riaz and Tchelepi, 2006). However, when the main part of the plume collapses this bottom part of the saturation profile becomes more important, see Figure 2. The leading part of the saturation profile keeps propagating with the same velocity, and the traveling wave at the bottom compensates for gas flow by propagating upward. Note that the speed of propagation of the bottom traveling wave exceeds V^*. Another interesting feature at this phase of plume evolution is that the saturation at the transition between the bottom rarefaction wave and the rarefaction wave of the leading part of the plume, S_R, becomes a function of time, $S_R = S_R(\tau)$. Hence, the velocity of propagation evaluated using Equation (11) also becomes a function of time. However, calculations (omitted in the present work) show that the variations of this velocity are small.

This plume configuration remains viable until the part of the saturation profile between the top and bottom traveling waves collapses. Once this happens, the saturation along the entire plume is close to the residual gas saturation. The plume continues to thin through the rarefaction wave at the bottom, Figure 3. Since the saturation of water exceeds S^*, the propagation of the top of the plume slows down dramatically. The theory suggests asymptotic thinning of the plume to the residual gas saturation.

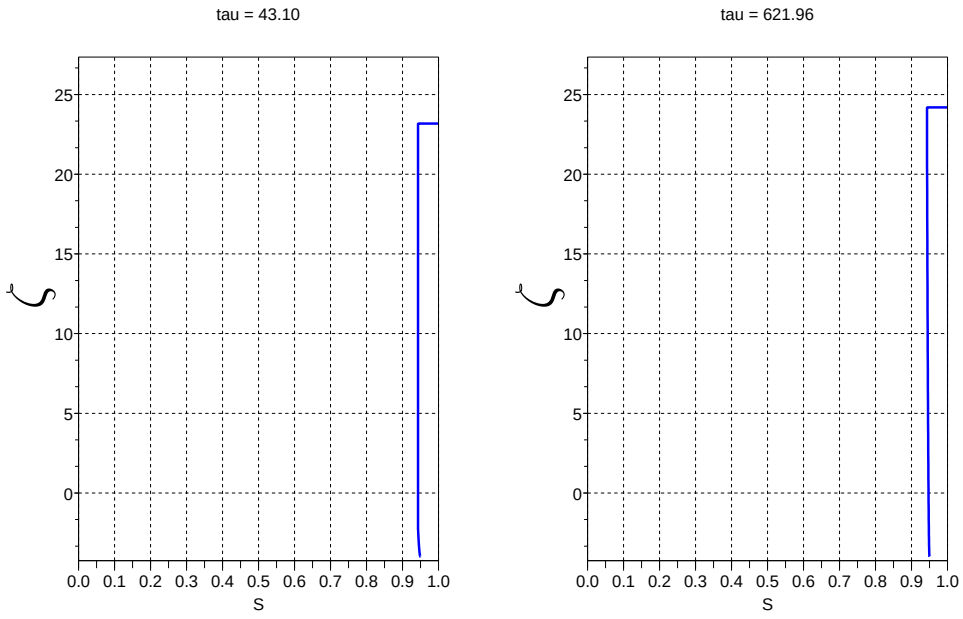

FIGURE 3. The final phase of plume evolution. The bottom rarefaction wave characterizes the saturation profile in most of the plume. The gas is closed to being trapped over the entire plume.

3.3. **Plume propagation in a heterogeneous formation.** The theory developed above assumes an idealized homogeneous formation. It is interesting to investigate the impact of heterogeneities on the speed of plume propagation. In this section, we consider a case where formation properties are variable with depth. To begin, consider the propagation of the leading top of the plume through an interface between two different rocks. Since the formation properties below and above the interface play a crucial role in the calculations, we will use dimensional values of the velocities. The subscript index $_1$ will denote the formation below the interface, and the index $_2$ will denote the formation above the interface. Thus, let ϕ_1 and k_1 characterize the porosity and permeability of the rock underneath the interface, and ϕ_2 and k_2 characterize the porosity and permeability of the rock above the interface. Let S_1 be the saturation at the top of the plume below the interface at the time of plume arrival. The Darcy velocity of gas immediately behind the plume top is given by

$$u_1 = \frac{k_1(\varrho_w - \varrho_g)g}{\phi_1 \mu_w} f_1(S_1) \tag{18}$$

When a shock in the saturation profile propagates, the discontinuity of Darcy velocity implied by the discontinuity in saturation is compensated by the velocity of propagation. This is the physical meaning of the Rankine–Hugoniot relationship at the front in two-phase flow. Unlike a shock, the boundary between two rock types does not move, so Darcy velocities on both sides of the interface must be equal:

$$\frac{k_1(\varrho_w - \varrho_g)g}{\phi_1 \mu_w} f_1(S_1) = \frac{k_2(\varrho_w - \varrho_g)g}{\phi_2 \mu_w} f_2(S_2) \tag{19}$$

Cancellation of similar factors on both sides of this equation eliminates the fluid parameters and leaves the rock properties only. Let a superscript asterisk denote the saturation corresponding to the maximum velocity of plume propagation, and a superscript ^{M} denote the maximum of the partial flow function:

$$\frac{f_i(S_i^*)}{1-S_i^*} = \max_S \frac{f_i(S)}{1-S}, \quad f_i(S_i^M) = \max_S f_i(S) \tag{20}$$

where i is either 1 or 2.

In mass balance equation (19), S_1 is the saturation at the tip of propagating plume. As we will see, it may be different from the saturation S_1^* corresponding to a homogeneous Medium 1. If Equation (19) is solvable with respect to S_2 for a given S_1, typically it has two solutions. since the plume propagates into a fully brine-saturated formation, only the larger value of S_2 is physically sensible.

First, let us consider a case where there is no S_2 satisfying mass balance equation (19). This happens in a case where the permeability of Medium 2 is insufficient to support the gas flow rate in Medium 1. Therefore, gas saturation will start growing at the interface and the flow rate will slow down correspondingly. The brine saturation in Medium 1 at the boundary will reach some value S_1', which is less or equal to S_1^*, so that the Darcy velocity in Medium 1 will match the maximum Darcy velocity in Medium 2:

$$\frac{k_1}{\phi_1} f_1(S_1') = \frac{k_2}{\phi_2} f_2(S_2^*) \tag{21}$$

Here, we have cancelled similar terms from Equation (19). We are interested in the smaller of two saturations S_1' satisfying Equation (21). This fluid rearrangement generates two shock waves on the saturation profile: an upward wave in Medium 2 with the velocity of propagation corresponding to S_2^*,

$$v_2^* = \frac{k_2(\varrho_w - \varrho_g)g}{\phi_2 \mu_w} \frac{f_2(S_2^*)}{1-S_2^*} \tag{22}$$

and a downward wave in Medium 1 with the velocity of propagation

$$v_1' = -\frac{k_1(\varrho_w - \varrho_g)g}{\phi_1 \mu_w} \frac{f_1(S_1^*) - f_1(S_1')}{S_1^* - S_1'} \tag{23}$$

The velocity v_1' is negative, since saturation $S_1' < S_1^*$ due to gas accumulation, and $f_1(S_1') < f_1(S_1^*)$ since this gas accumulation reduces the Darcy velocity in order to equalize it with the fluid flow in Medium 2, Figure 4.

Now, let the saturation S_1 be such that Equation (19) is solvable with respect to S_2. Then, there are two possibilities. If saturation S_2 evaluated from Equation (19) does not exceed S_2^*, $S_2 \le S_2^*$, then the gas supply is sufficient to support the maximum velocity of plume propagation in Medium 2. In such a situation, the plume will flow into Medium 2 with the theoretically maximal velocity described by Equation (22). The leading shock wave is followed by a rarefaction wave. The latter may or may not extend all the way to the stable point of maximal Darcy velocity, that is to the saturation S_2^M, Figure 5. If the arriving plume is so lean with respect to gas saturation, that the brine saturation S_2 evaluated from continuity equation (19) exceeds S_2^*, then the velocity of plume propagation in Medium 2 will be

$$v_2 = \frac{k_2(\varrho_w - \varrho_g)g}{\phi_2 \mu_w} \frac{f_2(S_2)}{1-S_2} < v_2^* \tag{24}$$

Thus, if the plume origin is separated from Medium 1 by a low-permeability layer, the fluid saturation at the tip of the plume must be greater than S_1^*, see Figure 6.

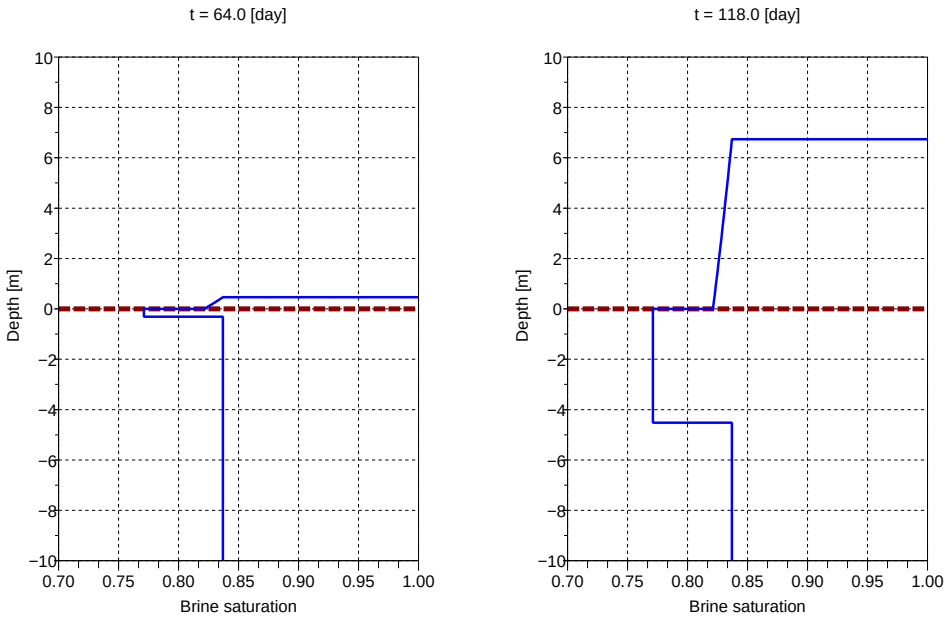

FIGURE 4. A plume crossing the boundary: the permeability of the formation above the interface is slightly lesser than that of the formation beneath the boundary (bold dashed line). A rarefaction wave behind the leading front is incomplete.

3.4. **Plume propagation in a heterogeneous formation.** Let us consider a formation of thickness H subdivided into zones with different properties. Inside each individual zone, the formation is assumed homogeneous. Let N be the total number of zones and H_i be the thickness of layer i, numbered in the direction of the plume propagation: from the bottom to the top. To evaluate the time of the plume crossing each layer, one needs to estimate the respective velocity v_i of the plume propagation. We do such an estimate using the results of the previous subsection.

In each layer, the velocity of plume propagation is either equal to the theoretical maximum, v_i^*, or is less than that if the underlying low-permeability layers reduce the actual velocity to a lower value. In the first case, the time of crossing the layer can be estimated upfront:

$$\tau_i^* = \frac{H_i}{v_i^*} = \frac{\phi_i \mu_w H_i}{k_i(\varrho_w - \varrho_g)g} \frac{1 - S_i^*}{f_i(S_i^*)} \tag{25}$$

If the maximal velocity of propagation is feasible in all sublayers, then the total time, T^*, can be determined by summation

$$T^* = \sum_i \frac{\phi_i \mu_w H_i}{k_i(\varrho_w - \varrho_g)g} \frac{1 - S_i^*}{f_i(S_i^*)} \tag{26}$$

This time can be treated as the theoretically minimal time of plume propagation.

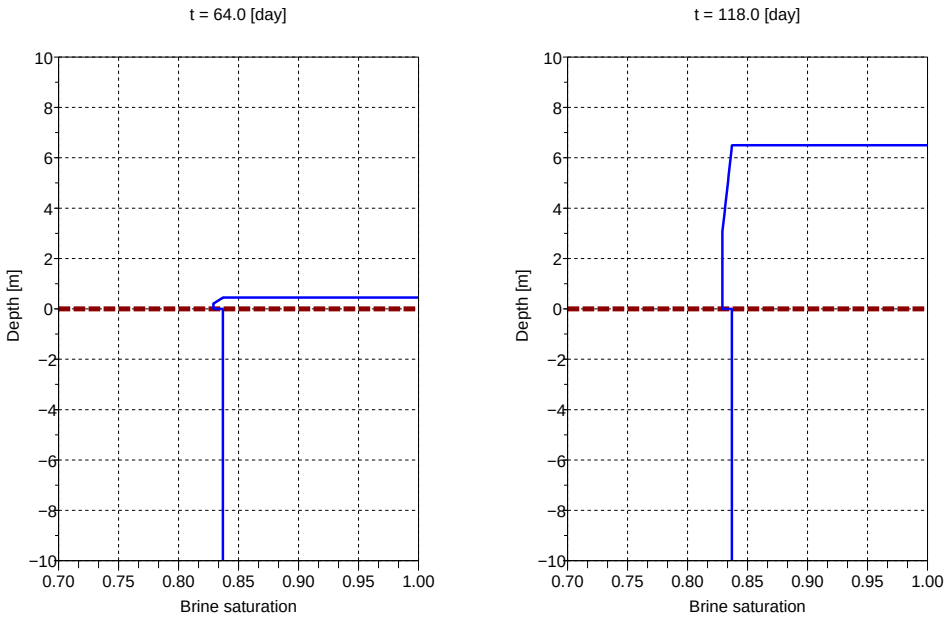

FIGURE 5. A plume crossing the boundary: the formation permeability above the interface is slightly less than that beneath the boundary (bold dashed line). The rarefaction wave behind the leading front is incomplete.

Now, let us consider a case where the maximal velocity of propagation is unfeasible in all layers. In such a case,

$$\tau_i = \frac{\phi_i \mu_w H_i}{k_i(\varrho_w - \varrho_g)g} \frac{1 - S_i}{f_i(S_i)} \tag{27}$$

where saturations S_i and S_{i+1} in two adjacent layers are related by the continuity equation (19). In particular,

$$f_i(S_i) = \frac{k_i \phi_{i-1}}{k_{i-1} \phi_i} f_{i-1}(S_{i-1}) \tag{28}$$

Repeatedly, using continuity equation (19), one gets

$$f_i(S_i) = \frac{k_i}{\phi_i} \frac{\phi_1}{k_1} f_1(S_1) \tag{29}$$

Hence, for τ_i, one obtains

$$\tau_i = \frac{\mu_w}{(\varrho_w - \varrho_g)g} \frac{\phi_1}{k_1} \frac{1 - S_i}{f_1(S_1)} H_i \tag{30}$$

After summation, the total travel time is

$$T = \frac{\mu_w}{(\varrho_w - \varrho_g)g} \frac{\phi_1}{k_1} \frac{1}{f_1(S_1)} (1 - \overline{S}) H \tag{31}$$

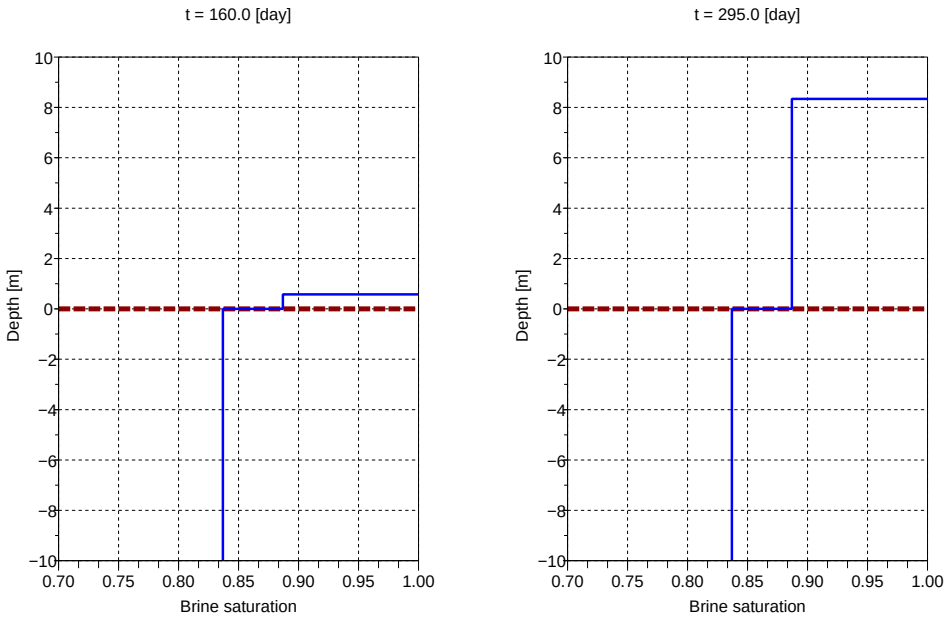

FIGURE 6. Lean plume behind the boundary: the gas supply below the boundary (bold line) is insufficient to support the maximum velocity of propagation above the boundary. The time elapsed between the shown saturation profiles is one month.

Here, $\overline{S}$ is the mean brine saturation:

$$\overline{S} = \sum_i (1 - S_i) \frac{H_i}{H} \tag{32}$$

This result relates the mean velocity of propagation of the plume in a heterogeneous formation, $\overline{v}$, to the mean brine saturation

$$\overline{v} = \frac{k_1(\varrho_w - \varrho_g)g}{\phi_1 \mu_w} \frac{f_1(S_1)}{1 - \overline{S}} \tag{33}$$

If permeability and porosity distributions $k(z)$ and $\phi(z)$ are known, and the dimensionless fractional flow function does not depend on depth, then, in case of non-maximal plume propagation velocity, the saturation distribution can be predicted on the basis of Equation (29):

$$S(z) = f^{-1}\left(\frac{k(z)}{\phi(z)} \frac{\phi_1}{k_1} f_1(S_1)\right) \tag{34}$$

This equation leads to an estimate of the mean saturation at the leading front of the plume and, respectively, to an estimate of the plume travel time.

3.5. **The impact of heterogeneity on plume propagation time.** Calculations in the previous section suggest the following rule of estimating the velocity of propagation when the plume crosses an interface between two media. Let us assume that the relative permeability curves are the same for the rock above

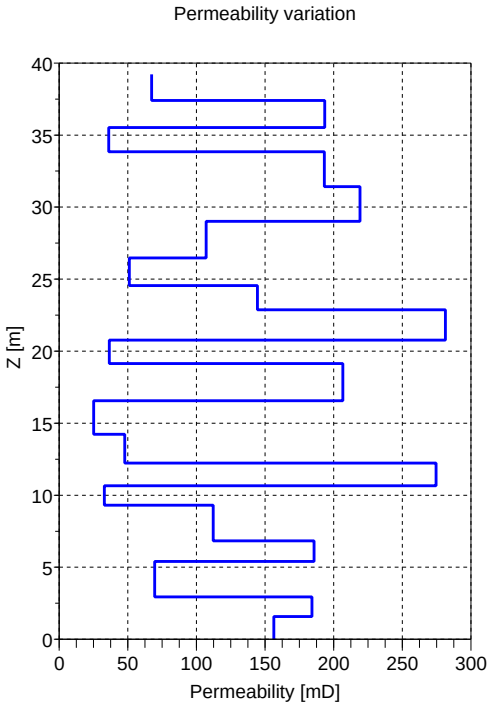

FIGURE 7. Vertical permeability profile.

and below the interface, so that one can use the same fractional flow function, $f(S)$. Then, water saturation at the leading front of the plume is always equal or exceeds S^*. If

$$f(S^*) \leq \frac{k_1\phi_2}{k_2\phi_1} f(S_1) \tag{35}$$

then $S_2 = S^*$ and the plume propagation speed in Medium 2 is at maximum. If the opposite inequality holds true, then S_2 must be determined from Equation (21), and Equation (24) determines the velocity of plume propagation. For illustration, consider a layered formation with the permeability distribution, which has been obtained with a random number generator, see Figure 7. Figure 8 shows plume propagation as a function of time accounting for the variations in permeability and ignoring it by using the harmonic mean permeability of all layers. In this example, the plume propagation is slowed down by the heterogeneity. The nature of this phenomenon is in the nonlinear dependence of the flow on fluid saturation. This result cannot be extended to a case of laterally heterogeneous formation. In that case, one should expect a faster plume propagation through a high-permeable path. For example, fractures can serve as natural conduits for a fast delivery of the leaking gas to the surface.

4. SUMMARY AND CONCLUSIONS

Buoyancy-driven viscous flow of a gas plume can be described approximately as one-dimensional two-phase countercurrent flow. This approximation is applicable to the flow far enough from the lateral

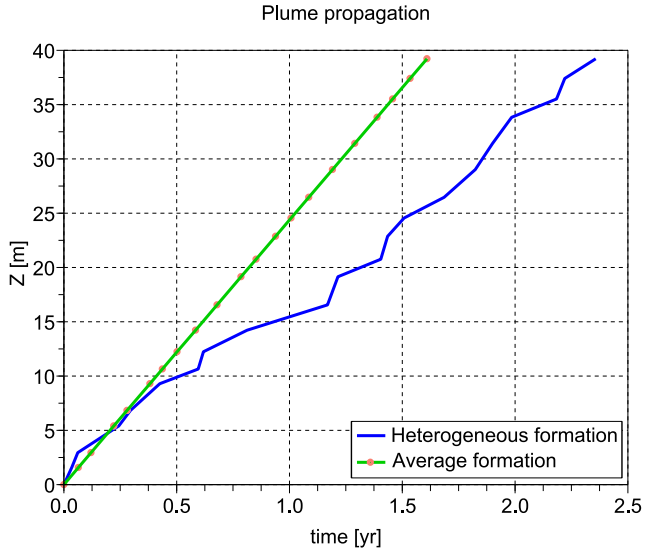

FIGURE 8. Vertical plume propagation versus time. The straight line shows propagation in a homogeneous formation with harmonic average permeability from the profile in Figure 7. The polygonal line has been calculated accounting for the heterogeneity. The circles are centered at the boundaries between the layers.

boundaries. In a vertical fracture or other laterally confined brine-saturated structure the flow also can be described as one-dimensional. Under certain conditions, the capillary effects can be neglected, which leads to a hyperbolic model of flow. The method of characteristics suggests two types of solutions: shock and rarefaction waves. In a porous medium, the gas plume does not flow like a bubble in bulk water. Instead, the leading part of the plume, having relatively low gas saturation propagates much faster than the main part of the plume. The saturation in the leading part of the plume can be estimated from the dimensionless fractional flow function. The velocity of propagation can be presented in a dimensionless form, which can be further scaled with a combination of rock absolute permeability and porosity, along with the densities and viscosities of the brine and gas.

The theory admits an extension to a heterogeneous aquifer. For a simple model of layered formation, it suggests rules of plume flow across an interface between two adjacent layers with different rock properties. The principal observation is that a single low-permeability layer dramatically reduces the plume propagation velocity in all overlaying strata. This observation follows from an estimate of the plume travel time. The travel time has been expressed in terms of the mean saturation over the whole thickness of interest and the minimal velocity of propagation. In an example with a random distribution of permeability variations, an increased plume travel time has been observed for all tried realizations. Therefore, an intact seal

plays a critical role in containment of injected CO_2 for a long time. A more comprehensive study of the impact of heterogeneity on plume propagation can be performed, combining the model proposed here with percolation-type simulations.

The character of the evolution of vertical saturation profile implied by the theory developed here suggests that a laterally-distributed plume should spread over the overlaying formation. To maximize the volume of trapped gas, it seems attractive to inject it at the bottom part of an aquifer in such a way that the plume spreads laterally as much as possible. Apparently, such injection pattern can be achieved by creation of horizontal fractures at the bottom of injection interval. However, such strategy may also increase risk of gas leakage if the plume reaches a fracture or a fault.

Acknowledgments

This work was supported by the U.S. Department of Energy's Assistant Secretary for Coal through the Zero Emission Research and Technology Program under US Department of Energy contract no. DE-AC02-05CH11231 to Lawrence Berkeley National Laboratory (LBNL). The authors a grateful to Dr. Andrea Cortis and Dr. Stefan Finsterle of LBNL for reviewing the manuscript and suggesting numerous improvements.

References

Al-Futaisi, A., Patzek, T. W., 2003. Impact of wettability on two-phase flow characteristics of sedimentary rock: Quasi-static model. Water Resources Research 39 (2), 1042–1055.

Buckley, S. E., Leverett, M. C., 1942. Mechanisms of fluid displacement in sands. Trans. AIME 146, 149–158.

Hubbert, M. K., 1956. Darcy's law and the field equations of the flow of underground fluids. Trans. AIME 207 (7), 222–239.

Juanes, R., Spiteri, E. L., Orr Jr., F. M., Blunt, M. J., 2006. Impact of relative permeability hysteresis on geologic CO_2 storage. Water Resources Research 42, W12418, doi:10.1029/2005WR004806.

Landau, L. D., Lifshitz, E. M., 1959. Course of Theoretical Physics. Fluid Mechanics. Vol. 6 of Series in advanced physics. Addison-Wesley, Reading, Mass.

Lax, P., 1973. Hyperbolic Systems of Conservation Laws and the Mathematical Theory of Shock Waves. Society of Industrial and Applied Mathematics, Philadelphia.

Muskat, M., 1949. Physical Principles of Oil Production. McGraw-Hill, New York, NY.

Petrovskii, I. G., 1966. Ordinary differential equations. Prentice-Hall, Englewood Cliffs, NJ.

Riaz, A., Tchelepi, H. A., 2006. Dynamics of vertical displacement in porous media associated with CO_2 sequestration. SPE paper 103169. In: 2006 SPE Annual Technical Conference and Exhibition. September 24–27, 2006. SPE, San Antonio, TX.

Silin, D., Patzek, T. W., Benson, S. M., September 2006. Exact solutions in a model of vertical gas migration. SPE paper 103156. In: 2006 SPE Annual Technical Conference and Exhibition. September 24–27, 2006. SPE, San Antonio, TX.

Silin, D., Patzek, T. W., Benson, S. M., 2007. A model of buoyancy-driven two-phase countercurrent fluid flow. Laboratory report LBNL-62607, Lawrence Berkeley National Laboratory, Berkeley, CA.

Valvante, P. H., Blunt, M. J., 2004. Predictive pore-scale modeling of two-phase flow in mixed-wet media. Water Resources Research 40, W07406, doi:10.1029/2003WR002627.

Lawrence Berkeley National Laboratory, 1 Cyclotron Road, MS 90-1116, Berkeley, CA 94720, USA
E-mail address: DSilin@lbl.gov

University of California, Berkeley, 425 Davis Hall, Berkeley, CA 94720, USA
E-mail address: patzek@patzek.berkeley.edu

Energy Resources Engineering Department, Stanford University, 074 Green Sciences Building, 367 Panama Street, Stanford, CA 94305-22020
E-mail address: SMBenson@stanford.edu